Contrast-enhanced XROMM reveals *in vivo* soft tissue interactions in the hip of *Alligator mississippiensis*

Henry P. Tsai, (iD) Morgan L. Turner, (iD) Armita R. Manafzadeh (iD) and Stephen M. Gatesy

Department of Ecology and Evolutionary Biology, Brown University, Providence, RI, USA

Abstract

Extant archosaurs exhibit highly divergent articular soft tissue anatomies between avian and crocodilian lineages. However, the general lack of understanding of the dynamic interactions among archosaur joint soft tissues has hampered further inferences about the function and evolution of these joints. Here we use contrast-enhanced computed tomography to generate 3D surface models of the pelvis, femora, and hip joint soft tissues in an extant archosaur, the American alligator. The hip joints were then animated using marker-based X-Ray Reconstruction of Moving Morphology (XROMM) to visualize soft tissue articulation during forward terrestrial locomotion. We found that the anatomical femoral head of the alligator travels beyond the cranial extent of the bony acetabulum and does not act as a central pivot, as has been suggested for some extinct archosaurs. Additionally, the fibrocartilaginous surfaces of the alligator's antitrochanter and femoral neck remain engaged during hip flexion and extension, similar to the articulation between homologous structures in birds. Moreover, the femoral insertion of the ligamentum capitis moves dorsoventrally against the membrane-bound portion of the medial acetabular wall, suggesting that the inner acetabular foramen constrains the excursion of this ligament as it undergoes cyclical stretching during the step cycle. Finally, the articular surface of the femoral cartilage model interpenetrates with those of the acetabular labrum and antitrochanter menisci; we interpret such interpenetration as evidence of compressive deformation of the labrum and of sliding movement of the menisci. Our data illustrate the utility of XROMM for studying *in vivo* articular soft tissue interactions. These results also allow us to propose functional hypotheses for crocodilian hip joint soft tissues, expanding our knowledge of vertebrate connective tissue biology and the role of joint soft tissues in locomotor behavior.

Key words: *Alligator*; cartilage; fibrocartilage; high walk; hip joint; hyaline cartilage; kinematics; ligamentum capitis femoris; menisci; XROMM.

Introduction

Members of Archosauria, the clade that includes crocodilians, birds, non-avian dinosaurs, pterosaurs, and other extinct forms, have evolved a wide diversity of limb morphologies and body sizes. Among the two extant groups, the distinctive terrestrial locomotor styles of crocodilians (plantigrade quadrupeds with variably adducted posture) and birds (digitigrade bipeds with fully erect posture) are reflected in their highly disparate hind limb musculoskeletal anatomies (Huxley, 1870; Romer, 1923; Galton, 1969; Parrish, 1987a,1987b; Gatesy & Middleton, 1997; Wilson & Carrano, 1999; Hutchinson, 2001a, 2001b; Maidment & Barrett, 2012; Benson & Choiniere, 2013) and joint architectures (Kuznetsov & Sennikov, 2000; Bonnan et al. 2010; Holliday

et al. 2010; Tsai & Holliday, 2015; Tsai et al. 2018). For example, the avian hip joint exhibits relatively thin layers of articular soft tissues at skeletal maturity. Such high bony congruence in birds has allowed workers to use the osteological morphologies of the femur and the acetabulum as proxies for *in vivo* surface geometry when describing hip articulation (Rubenson et al. 2007), kinematics (Kambic et al. 2014, 2015), and loading (Goetz et al. 2008). In contrast, the crocodilian hip joint retains thick layers of articular soft tissues throughout life (Gadow, 1901; Bonnan et al. 2010; Fujiwara et al. 2010; Holliday et al. 2010). Accordingly, the shape and size of femoral and acetabular articular surfaces differ significantly from those of the underlying bony elements (Holliday et al. 2010; Tsai & Holliday, 2015). Kinematic analyses of crocodilian hind limbs based on external markers (Reilly & Elias, 1998) and X-ray imaging (Brinkman, 1980; Gatesy, 1991) have not been able to visualize dynamic joint surface relationships. Therefore, our current knowledge of the role articular soft tissues play in maintaining joint congruence, influencing range of motion, and transmitting locomotor forces is limited.

Correspondence

Henry P. Tsai, Department of Biomedical Sciences, Missouri State University, Springfield, MI 65897, USA. E: HTsai@missouristate.edu

The crocodilian condition is of critical paleobiological interest because many extinct archosaurs have highly incongruent bony hip joints as well (Tsai et al. 2018). Frequent presence of osteological correlates for thick layers of articular soft tissues on well-preserved archosauromorph fossils, such as those of pseudosuchians (e.g. Sawin, 1947; Nesbitt, 2011; Lacerda et al. 2016), sauropods (e.g. Marsh, 1896; Hay, 1908; Bonnan, 2004), and large ornithischians (e.g. Gilmore, 1914; Lehman, 1989; Dilkes, 2001), suggests that these structures played crucial roles in hip joint function in both the crocodilian and avian lineages. Several workers have therefore suggested that anatomical descriptions of bony morphology are likely insufficient for understanding articular geometry in life (Osborn, 1898; Coombs, 1975; Holliday et al. 2010). Insights into the functional relationship between hip movement and soft tissue interactions in crocodilians will improve our ability to reconstruct hind limb posture in extinct archosaurs and will broaden our understanding of how articular tissues evolved in vertebrates.

Extant archosaurs share homologous regions of articular soft tissues with other living diapsids (Tsai & Holliday, 2015) and extinct archosaurs (Tsai et al. 2018). In both birds and crocodilians, the proximal femoral surface is composed of a core of hyaline cartilage surrounded by a sleeve of fibrocartilage. The sub-spherical avian femoral head is augmented by a saddle-shaped articular surface (*facies articularis antitrochanterica*, Baumel & Raikow, 1993) of the femoral neck. The entire proximal end of the femur of crocodilians is convex, such that the surfaces considered homologous with the head and *facies articularis antitrochanterica* are continuous. In birds and crocodilians, the acetabulum is composed of a hyaline cartilage-covered cranial portion, a fibrous acetabular labrum on the supraacetabulum (the 'ceiling'), and a fibrocartilaginous antitrochanter in the caudal region (Tsai & Holliday, 2015). The avian acetabulum possesses a small labrum and a laterally expanded antitrochanter with a single fibrocartilaginous surface. In contrast, the crocodilian acetabulum exhibits a large, pliant labrum and an antitrochanter made of two semilunate menisci (Tsai & Holliday, 2015). When articulated, the spherical avian femoral head acts as a pivot within the acetabular socket (Hertel et al. 2007). A secondary articulation, the *facies articularis antitrochanterica* of the femoral neck, is thought to engage with the antitrochanter to prevent femoral abduction (Hertel et al. 2007). However, the dynamic relationship between the anatomical homologues of these structures in crocodilians remains unknown.

In the present study, we qualitatively describe the 3D kinematics of the crocodilian hip joint during forward terrestrial locomotion. We used biplanar X-ray imaging to record juvenile *Alligator mississippiensis* performing continuous strides of high walking on a motorized treadmill. We then reconstructed the 3D positions and orientations of the cartilaginous articular surfaces of the proximal femur relative to the soft tissues of the acetabulum using a combination of marker-based XROMM (X-ray Reconstruction of Moving Morphology, Brainerd et al. 2010) and contrast-enhanced computed tomographic (CT) techniques (Gignac et al. 2016; Pauwels et al. 2013). We describe the dynamic interactions among hip joint soft-tissue surfaces in alligators, and discuss the implications of our findings for reconstructing joint articulation and locomotion in extinct archosaurs.

Materials and methods

Three female American alligators, *Alligator mississippiensis*, were acquired from the Rockefeller Wildlife Refuge (Grand Chenier, LA, USA) as eggs and captive-raised at the alligator colony at California State University, San Bernardino (San Bernardino, CA, USA). The alligators were kept in 122-gallon fiberglass tanks, with enclosure temperature maintained between 25 and 30 °C throughout the year, and fed on a diet of commercially available alligator feed (LoneStar Alligator chow pellets, 50% protein by weight) approximately twice a week, *ad libitum*, until reaching 3 years of age (100–150 cm total length). At the time of the surgery, animal 1 weighed 3.82 kg; animal 2 weighed 3.80 kg, and animal 3 weighed 3.6 kg. At Brown, the animals were kept in 1741-liter tank enclosures, with water temperature maintained at 25–30 °C, fed dead mice and LoneStar pellets twice weekly, and allowed free access to water and basking platforms. All surgical and experimental procedures involving live animals were approved by the Institutional Animal Care and Use Committee at Brown University.

We used marker-based XROMM techniques (Brainerd et al. 2010) to track the 3D translations and rotations of the pelvis and femora during locomotion. The animals were sedated with butorphanol with body temperature controlled using a circulating water heating pad; anesthesia was induced and maintained using isoflurane. Conical markers (0.8 mm diameter and ~ 2.5 mm long) fashioned from carbide steel rods were manually inserted into bones using a pin vise (see Kambic et al. 2014 for fabrication details). Pelvic markers (five) were implanted into the pre- and post-acetabular crests of both ilia, as well as in the ischial symphysis. Each femur received three to four markers placed into the medial and lateral sides of the proximal metaphysis and distal femoral condyles (Fig. 1A). Additional markers were implanted in bones distal to the femur but are not used in this study. Animals were given ketoprofen as an analgesic agent during post-surgical recovery, and given a week to recover before locomotor trials.

Locomotor trials were conducted in the W. M. Keck Foundation XROMM Facility at Brown University. Alligators were trained to walk on a motorized treadmill (Jog-a-Dog model DC5, JOG A DOG; LLC, Ottawa Lake, MI, USA) outfitted with custom-made acrylic walls to create a 35-cm-wide × 148-cm-long × 48-cm-high chamber. Treadmill speed was adjusted to keep the animal's hind limbs within the X-ray field of view. Animals were imaged using two Varian model G-1086 X-ray tubes (80 kV, 100 mA, magnification level 0) and two Dunlee model TH9447QXH590 image intensifiers (40.64 cm diameter) mounted on mobile-arm bases at source-image distances of 134–136 cm. Phantom v10 high-speed cameras (Vision Research, Wayne, NJ, USA) recorded at 100 fps, 1/2000 s shutter speed, and 1760 × 1760 pixel resolution. Images of a standardized metal distortion grid (Brainerd et al. 2010) and a Lego-based calibration cube (Knörlein et al. 2016) were recorded before and after each session. We conducted more treadmill trials than the final
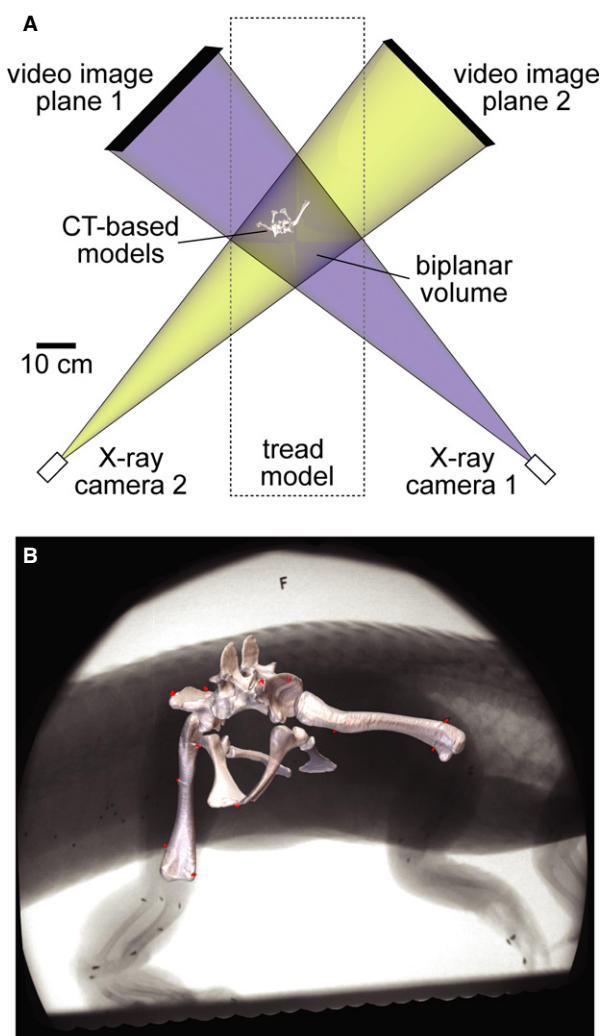
Fig. 1 XROMM setup reconstructed as a MAYA scene. (A) Top view of treadmill representing the two X-ray systems as pairs of virtual X-ray cameras and video image planes. The blue and yellow beams overlap in the biplanar volume, allowing bone and soft tissue models to be animated based on the rigid body transformations of marker clusters. (B) Models of the pelvis and femora registered to X-ray Video S1 showing the locations of surgically implanted conical markers (red).

number of trials analyzed using XROMM to ensure observation of consistent, representative high walk behaviors. A total of seven locomotor trials consisting of 10 strides were analyzed for animal 1. A total of four trials consisting of 10 strides were analyzed for animal 2. A total of six trials consisting of 17 strides were analyzed for animal 3. After kinematic data collection was completed, animals were euthanized by intraperitoneal injection of beuthanasia after isoflurane induction.

Bone and cartilage surface model construction

Cadaveric specimens of the three experimental animals were dissected to extract cartilage-capped hind limb skeletal elements. After removal of skin and muscles, the sacrum was removed by disarticulation from the last dorsal and the first caudal vertebrae. All pelvic joints were left intact. The femora were disarticulated from the acetabulum by incising the synovial capsule, including the iliofemoral ligament. The *ligamentum capitis femoris* (L. cf) was incised close to its insertion onto the femur such that the majority of this ligament, including its pubofemoral and ischiofemoral crura, was preserved in the acetabulum.

The freshly disarticulated, cartilage-capped limb bones were immediately scanned using a FIDEX Multi-Modality Veterinary CT Scanner (Animage; LLC, Pleasanton, CA, USA) at 110 kV, 0.08 mA, 480 × 480 resolution, and 0.173 mm slice thickness. This initial scan digitized the overall shape and volume of bony tissues and joint soft tissues in each limb segment but was unable to differentiate between soft tissue types (e.g. hyaline- and fibrocartilage). Subsequently, the cartilage-capped bones were fixed in 10% neutral buffered formalin, then stored in 70% ethanol, before undergoing saturation by contrast-enhancing media to increase visual distinction between joint soft tissues in CT imaging. All hind limb elements except for the right femur of animal 3 were stained for 1 week in 5% phosphomolybdic acid (PMA) following an overnight pretreatment in a sucrose solution using techniques modified from Pauwels et al. (2013). The right femur of animal 3 underwent 4 weeks of saturation via Lugol's Iodine (I2KI) using techniques modified from Metscher (2009), Jeffery et al. (2011), and Tsai & Holliday (2011) in order to compare the effectiveness of both treatments in tissue-specific staining. The specimens were then CT-imaged using the same FIDEX scanner and settings as the initial, freshly dissected scans. The two staining modalities produced comparable results in tissue-specific contrast.

CT data were exported as DICOM files and imported into AMIRA v5.2 (Visage Imaging, San Diego, CA, USA) for reconstruction. Osseous and soft tissue structures of the pelvis and femora were differentiated using a combination of manual outline segmentation and threshold segmentation techniques, producing surface models reflective of their *ex vivo* shape (Figs 2 and 3). Visual comparison between 3D models of the formalin-fixed, contrast-stained soft tissues showed no discernable difference in soft tissue shape from to their earlier, freshly dissected counterparts, suggesting a negligible amount of tissue shrinkage during the fixation and staining process. The surface models were exported as 3D surface models (.obj files) and imported to (V12; Geomagic, Inc. Morrisville, NC, USA), where non-biological imaging artifacts created by the carbide markers were repaired. The cartilage-capped proximal femoral models were then divided into sets of surface patches based on two soft tissue types (fibrocartilage and hyaline cartilage surfaces) identified based on CT contrast, and three anatomical regions (femoral head, femoral neck, and L. cf insertion) based on regional anatomy and homology (Fig. 2). In particular, the femoral neck is here defined as the region on the proximal femur between the femoral head and the greater trochanter. Bone and soft tissue surface models were imported into MAYA 2014 and 2016 (Autodesk Inc., San Rafael, CA, USA).

XROMM animation

XMALab (versions 1.2.10 – 1.5.0; Knörlein et al. 2016) was used to undistort video, calibrate cameras, and track markers. We evaluated precision of tracking (see Brainerd et al. 2010) by taking the mean of the standard deviations of intermarker distances for 9–13 co-osseous marker pairs per trial (over 4142 frames representing seven trials (two trials from animal 1, two trials from animal 2, and three trials from animal 3) were collected from three individuals). The mean standard deviation for 83 total pairwise intermarker distances

Fig. 2 Articular surface models of femoral soft tissues as reconstructed by contrast-enhanced CT scans. (A,F) Longitudinal and axial CT sections of a right proximal femur, respectively, after 2 weeks in 5% PMA. (B,D, G) 3D model of the proximal femur in medial, lateral, and proximal views, respectively, color-coded by soft tissue. Blue and green spheres represent the particle emitters, traced in Fig. 4. (C,E,H) 3D model of the proximal femur in medial, lateral, and proximal views, respectively, color-coded by anatomical region. Gray signifies unassigned parts of the articular surface. Scale bar: 10 mm. fc, fibrocartilage (light green); fh, femoral head (blue); fm, femur (tan); fn, femoral neck (dark green); hc, hyaline cartilage (cyan); I.lcf, insertion of ligamentum capitis femoris (orange); mk, bone marker; troch, greater trochanter.
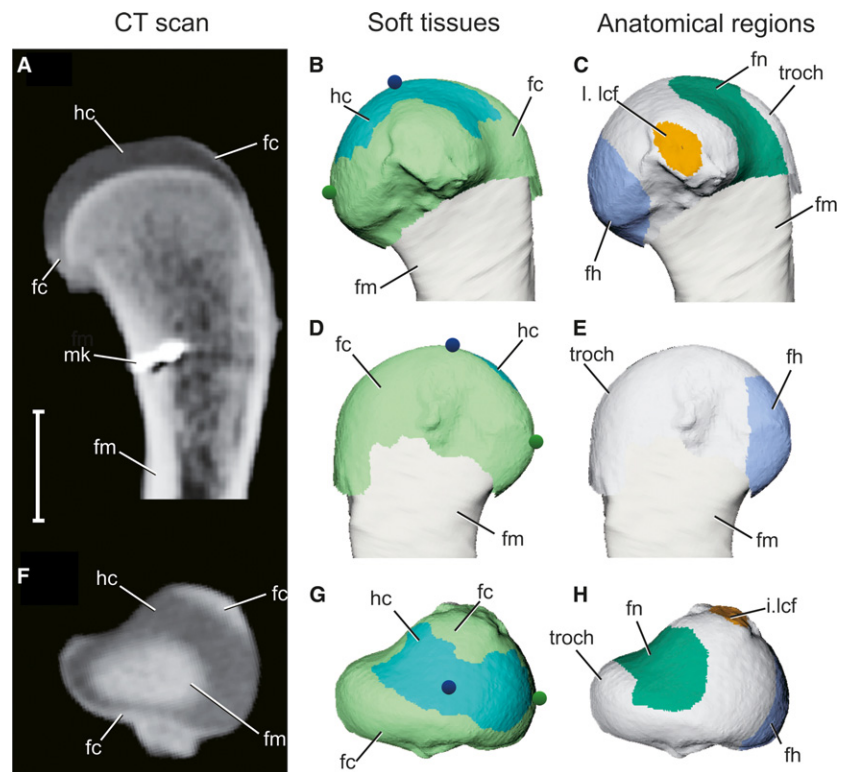
yielded an overall precision of 0.197 mm. Reconstructed 3D marker coordinates were combined with CT-derived marker centroids in XMALab to calculate pelvic and femoral rigid body transformations, which were then filtered using a low-pass Butterworth filter at 10 Hz. Rigid body transformations from multiple trials of high walking were concatenated for each individual by combining the rigid body transformations from multiple trials chronologically into a single file. The concatenated rigid body transformations were then applied to the pelvic and femoral bone models to reconstruct the 3D positions of each element within the experimental scene in Maya (Fig. 1B). Articular soft tissue element models were connected to their skeletal segments, such that they followed the movements of their respective bony elements. Each tissue type and anatomical region was given a color-coded shader following the convention of Tsai & Holliday (2015).

The 3D motion of the alligator hip is here described by characterizing the movement of the femur relative to the acetabulum. To set up a repeatable pelvic orientation among individuals, we created a coordinate system following Kambic et al. (2014). In Geomagic Studio, we fit a sphere to each acetabulum (including soft tissue models) and a cylinder to the centra of the two sacral vertebrae. The centroids of the acetabular spheres were connected to make a transverse axis, which was crossed with a longitudinal axis from the vertebral cylinder to establish the third, dorso-ventral axis. We then stabilized the pelvis at the origin of the Maya workspace by applying the inverse transforms of the pelvic animation to the pelvic and femoral models. By removing all pelvic yaw, pitch, roll and translations, a fixed acetabular reference frame for femoral movement was established.

We visualized the dynamic relationships between gross motion of the entire femur and the relative excursions among femoral and acetabular articular surfaces using two methods within Maya. First, we created small, spherical shapes (particles) to act as motion path

tracers. We attached particle emitters to three locations on the femur model, specifically the proximal terminal apex of the hyaline cartilage, the cranial apex of the fibrocartilage on the anatomical femoral head, and the distal intercondylar groove. The proximal apex was identified as the most distant point from the distal intercondylar groove on the hyaline cartilage surface of the proximal femur, whereas the cranial apex was identified as the cranial-most extent of the hyaline-fibrocartilage junction on the anatomical femoral head. Each emitter acted like a 3D stylus, leaving behind one particle per frame to form a particle stream as it traveled relative to pelvic structures. The colors of the particles are based on the femoral tissues and regions that they are meant to represent (e.g. dark blue for the proximal terminal apex of the hyaline cartilage in Fig. 2B, 2G). Because the particles are emitted at a regular rate, the more closely spaced regions along the particle stream signify slower movement of the femur during the step cycle, and vice versa.

Second, we mapped the 3D locations of surface patches representing femoral soft tissues and anatomical regions relative to the acetabulum. We tracked the locations of femoral surface patches during the step cycle by creating a duplicate patch model at each frame of the animation using the Animation Snapshot tool in Maya. This method creates a set of stroboscopic patch traces – an aggregate record of the 3D positions and orientations assumed by femoral surfaces relative to the acetabulum during a stride.

Results

Articular soft tissue reconstruction

Contrast-enhanced computed tomography was able to distinguish fibrocartilage, hyaline cartilage, and bone as distinct grayscale values, allowing segmentation of the
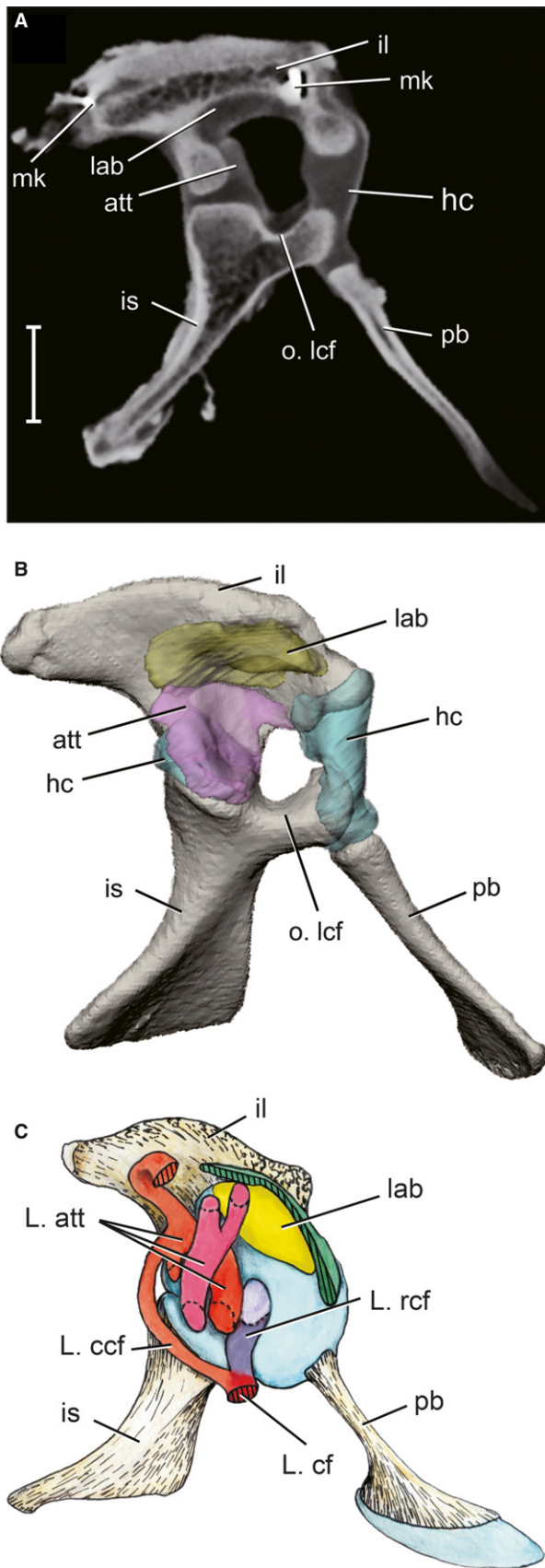
Fig. 3 Articular surface models of acetabular soft tissues as reconstructed by contrast-enhanced CT scans. (A) Parasagittal CT section of a right pelvis after 2 weeks in 5% PMA. (B) 3D model of the pelvis in right lateral view, color-coded by soft tissue. Scale bar: 10 mm. att, antitrochanter (pink); hc, hyaline cartilage (blue); il, ilium (tan); is, ischium (tan); lab, acetabular labrum (yellow); mk, bone marker; o.lcf, origin of ligamentum capitis femoris; pb, pubis (tan).

alligator hip joint tissues as 3D surface models (Figs 2 and 3). The raw CT data are consistent with anatomical data previously obtained via dissection, histology, and DiceCT imaging of the alligator hip joint (Tsai & Holliday, 2015). Anatomical abbreviations are summarized in Table 1.

The acetabulum possesses three distinct articular surfaces: a cranioventral hyaline cartilage portion surrounding the pubo-iliac joint (aqua in Fig. 3B); a pliant, fibrous acetabular labrum along the acetabular 'ceiling' (yellow in Fig. 3B); and a set of overlapping menisci that comprises the antitrochanter on the caudal portion of the acetabulum (purple in Fig. 3B). The medial wall of the acetabulum is unossified and forms an inner acetabular foramen, covered by an acetabular membrane during life. The ventral rim of the inner acetabular foramen provides the origin of the *rostral ligamentum capitis* (L. rcf), which is the dominant component of the *ligamentum capitis femoris* (L. cf). The insertion of L. cf is located between the femoral head and the medial protuberance on the proximal femur. The acetabular origin is noted on the acetabular 3D models (Fig. 3B), whereas the femoral insertion of L. cf (orange) is mapped onto femoral 3D models (Fig. 2C, 2H). However, the ligament itself is not reconstructed as a 3D model because it was incised in order to disarticulate the hip joint for CT scanning.

The proximal femur is composed of a core of hyaline cartilage (light blue in Fig. 2B, 2G), which attaches to the calcified cartilage-covered growth plate surface. Surrounding

Table 1 Anatomical abbreviations.

Abbreviation	Anatomical nomenclature
att	Antitrochanter
fc	Fibrocartilage
fh	Femoral head
fm	Femur
fn	Femoral neck
hc	Hyaline cartilage
il	Ilium
i. lcf	Insertion of *ligamentum capitis femoris*
is	Ischium
lab	Acetabular labrum
L. cf	*Ligamentum capitis femoris*
L. ccf	Caudal *ligamentum capitis femoris*
L. rcf	Rostral *ligamentum capitis femoris*
o. lcf	Origin of *ligamentum capitis femoris*
pb	Pubis
troch	Greater trochanter

the hyaline core is a sleeve of fibrocartilage (light green in Fig. 2B, 2G), which attaches distally to a raised shelf of longitudinally striated cortical bone, termed the metaphyseal shelf. The fibrocartilage sleeve extends proximally to partially enclose the hyaline cartilage layer, as well as distally where it merges into the periosteum (Tsai & Holliday, 2015). Because the articular surface of the proximal femur consists of both fibro- and hyaline cartilage regions, anatomical structures of the proximal femur may possess either or both tissue types as described below.

The anatomical femoral head (dark blue in Fig. 2C, 2H) is a craniomedially oriented tuber on the proximal femur (Hutchinson, 2001b; Nesbitt, 2011). The anatomical femoral head is composed of a hyaline cartilage proximal portion but also includes part of the metaphyseal fibrocartilage sleeve on its distal extent. The crocodilian femoral neck (dark green in Fig. 2C, 2H) is here used to denote the region on the proximal femur between the femoral head and the greater trochanter, a region termed the *facies articularis antitrochanterica* by Baumel & Witmer (1993) and Hutchinson (2001b). The articular surface of the femoral neck is composed of a hyaline cartilage surface on its apical portion, but also includes part of the fibrocartilage sleeve at the metaphyseal boundary (Fig. 2C, 2H).

In freshly dissected cadaveric specimens, manipulations reveal that the acetabular labrum is deformable and the antitrochanter menisci are mobile. The labrum's pliability is likely due to its fibrous tissue composition, whereas the menisci's mobilities reflect their intracapsular ligamentous attachments. However, because the hip joints were disarticulated as part of the staining preparation, the segmented 3D models of these soft tissues represent their shapes in an unloaded state. The models are reconstructed as static objects and therefore do not deform during animation. Similarly, because the L. cf was incised close to its femoral insertion, the majority of this ligament remains on the ventral acetabulum. Although the L. cf itself is not reconstructed as a 3D model, its motion was visualized by observing the motion trail left by the insertion of L. cf relative to its origin.

Hip kinematics

Rather than presenting hip kinematics using traditional graphs of joint angles (Gatesy, 1991; Reilly & Elias, 1998), we qualitatively describe alligator femoral motion during the high walk by tracing the motion paths of particles emitted from three locations on the models' surfaces (Fig. 4). During each step cycle, particles left by the distal emitter trace out a 3D loop. In lateral view, the right femoral trace is semilunar in shape, with sequential poses progressing in a clockwise direction (Fig. 4A). In caudal view, the loop is

Fig. 4 Dynamic relationship between the femur and pelvis during high-walking, visualized using particle traces. (A,C,E) The motion path of a distal femoral particle (red) over four strides in right lateral, caudal, and ventral views, respectively. (B,D,F) The motion paths of the terminal apex of the femur (blue) and cranial apex of the femoral head (green) in magnified lateral, caudal, and ventral views, respectively (see Fig. 2) for one stride, corresponding to the bright red distal particle path. Paths are shown both in acetabular context and offset for visibility, with portions of the proximal femoral paths that interpenetrates with acetabular structures illustrated by the lighter shadings and dotted outlines. Gray-scale arrows alongside motion paths denote directionality of movement (dark to light). Four positions during the high walk sequence (1, maximum hip flexion at approximate heel strike; 2, maximum hip adduction at approximate mid-stance; 3, maximum hip extension at approximate toe-off; 4, maximum hip abduction at approximate mid-swing) are indicated throughout (unnumbered poses are occluded by bone). Scale bars: 1 cm.
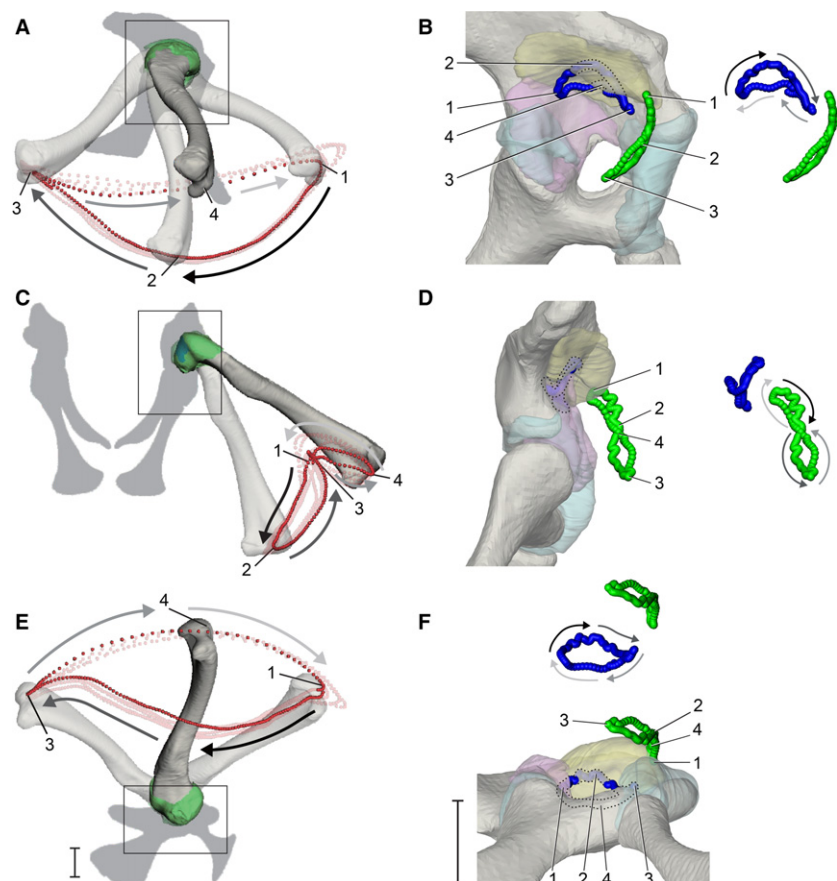
compressed into an oblique B-shape that is traversed in a counterclockwise direction (Fig. 4C). In ventral view, the clockwise loop is spindle-shaped (Fig. 4E). Four femoral positions along the particle loop were used to describe extremes of hip motion during the step cycle. With each stride, the distal femur traverses the loop from maximal hip flexion just prior to the swing-stance transition (Fig. 4, position 1), to maximal hip adduction near mid stance (position 2), to maximal extension in latest stance (position 3), to maximal abduction near mid swing (position 4), before returning to position 1.

We describe the kinematics of the proximal femur using particles emitted from the terminal apex (blue) and the cranial apex of the femoral head (green) (Fig. 4B,44). Overall, the terminal apex traces a miniature version of the distal particle loop, rotated *ca.* 180° about the animal's dorsoventral body axis. In lateral view, the semilunar loop is still traversed in a counterclockwise direction each stride but is concave ventrally (Fig. 4B). Just prior to foot contact, the terminal apex is located at its caudal-most point on the particle loop (position 1). As the femur undergoes coupled adduction and extension during early stance, the terminal apex moves craniodorsally until mid-stance (position 2). During late-stance, the terminal apex moves cranioventrally until it reaches the cranial-most point on the particle loop (position 3). As the femur undergoes coupled abduction and flexion during early swing, the terminal apex moves caudomedially until it reaches mid-swing (position 3), after which it moves caudolaterally during late-swing and returns to the beginning for the next heel strike. The shapes and directions of the terminal apex trace in caudal and ventral views (Fig. 4D,4) are correspondingly rotated in the opposite direction relative to the distal trace (Fig. 4C,4). Such inversions result from the hip's
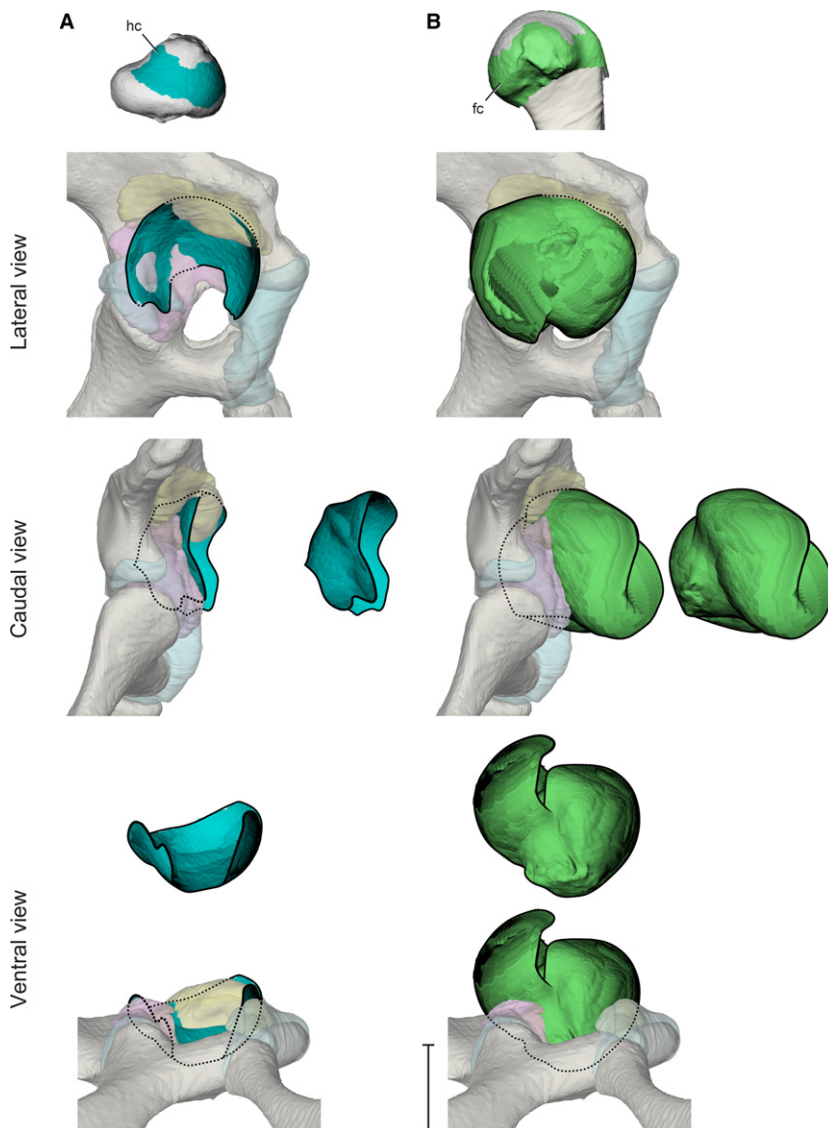
Fig. 5 Stroboscopic patch traces of the 3D positions and orientations assumed by femoral cartilaginous surfaces (top) relative to the acetabulum during a typical high-walking stride. (A) Hyaline cartilage in lateral, caudal, and ventral views. (B) Fibrocartilage in lateral, caudal, and ventral views. Paths are shown both in acetabular context and offset for visibility. Scale bar for acetabular views: 1 cm.
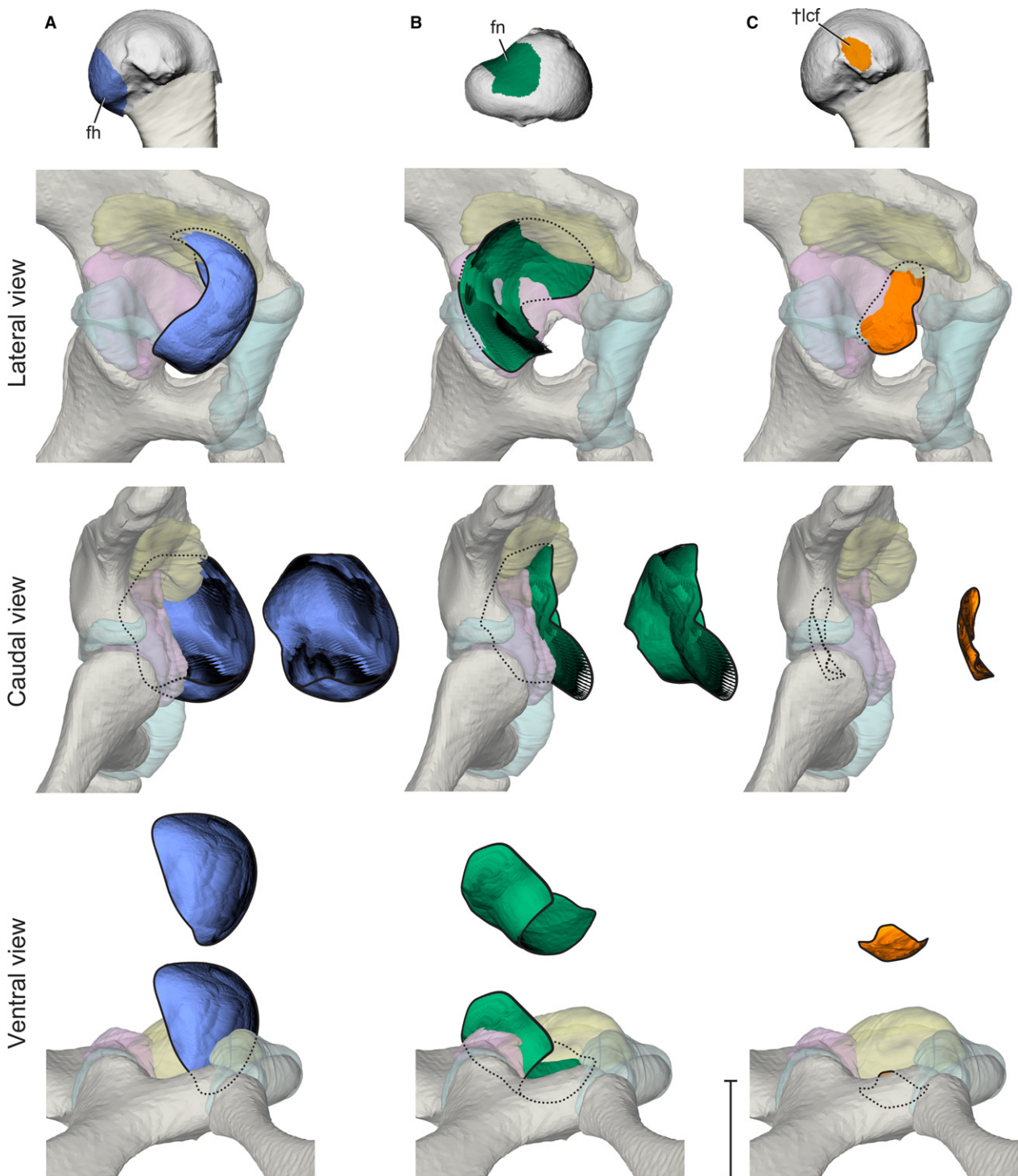
Fig. 6 Stroboscopic patch traces of the 3D positions and orientations assumed by femoral anatomical regions (top) relative to the acetabulum during a typical high-walking stride. (A) Femoral head in lateral, caudal, and ventral views. (B) Femoral neck in lateral, caudal, and ventral views. (C) Ligamentum capitis insertion in lateral, caudal, and ventral views. Paths are shown both in acetabular context and offset for visibility. Scale bar for acetabular views: 1 cm.

instantaneous rotation axes being located within the proximal femur rather than on or superficial to its articular surface. It is noteworthy that as the femur approaches and exits mid-stance phase (positions 1–3 in Fig. 4), and the terminal apex interpenetrates with the 3D surface of the acetabular labrum model (see Discussion).

The trace of the cranial apex of the femoral head forms an elongated, caudally concave 'figure 8' loop near the cranial edge of the acetabulum. In caudal view (Fig. 4D), the cranial apex starts at the top of the 'figure 8' (position 1, heel strike) and moves clockwise ventrally as the femur undergoes extension and adduction to mid stance (position 2). The cranial apex path undergoes an inflection to the counterclockwise direction shortly after passing position 2, and moves dorsally again upon nearing toe-off (position 3). Finally, the cranial apex continues moving counterclockwise until the femur arrives at mid-swing (position 4), where its particle path again inflects to move clockwise until reaching the next footfall.

The cranial apex particle trace shows that the femoral head exits the soft tissue extent of the acetabulum ventrolaterally, as delineated by both bone and articular soft tissues, during the stance phase of each step cycle. The particle then reenters the acetabulum dorsomedially during the swing phase, such that the femoral head is only located within the acetabulum as the femur approaches and exits heel-strike (around position 1). Lastly, the cranial apex trace interpenetrates with the 3D surface of the acetabular labrum near position 1, similar to the behavior of the terminal apex near position 2 (mid-stance).

Acetabular and femoral tissue contacts

During the high walk, the hyaline cartilage articular surface of the proximal femur follows the basic trajectory of the terminal apex particle, moving cranially within the acetabulum during the stance phase and caudally during the swing phase. Overall, the path traveled by the hyaline cartilage surface closely matches the shape of the soft tissue acetabulum (Fig. 5A). As the femur approaches mid-stance, the hyaline cartilage surface consistently penetrates the ventral surface of the labrum model (see Discussion). At no point during the step cycle does the hyaline cartilage surface impinge upon the inner acetabular foramen. The cranial-most portion of the hyaline cartilage surface exits the acetabulum during late stance through early swing, but for most of the step cycle the hyaline cartilage surface remains within the acetabulum.

The metaphyseal fibrocartilage sleeve covers a greater fraction of the exposed proximal femoral articular cartilage. During the high walk, femoral fibrocartilage sweeps out a substantial ellipsoid (Fig. 5B) that obscures the entire articular surface of the acetabulum in lateral view.

Acetabular and femoral regional contacts

The anatomical femoral head of *Alligator* undergoes substantial movement outside the acetabulum during high walking, and roughly follows the path of the cranial apex particle (Fig. 6A). As the femur extends during the stance phase, the femoral head moves ventrolaterally along the cranial edge of the acetabulum. The femoral head only approaches the interior of the acetabulum during postures in which the hip is maximally flexed from late swing into early stance.

During the swing phase, the femoral neck glides ventrolaterally across the caudal portion of the acetabulum, and maintains surface contact with the antitrochanter as the femur protracts (Fig. 6B). When the hip reaches its most flexed posture (position 1), the antitrochanter contacts the most proximal, hyaline cartilage portion of the femoral neck. As the femur extends during the stance phase (position 1–3), the femoral neck moves dorsomedially and enters deeper into the acetabulum, simultaneous with the ventrolateral movement of the femoral head out of the acetabulum. At no point during the step cycle does the femoral neck disengage from the antitrochanter menisci.

The insertion, or femoral attachment, of *ligamentum capitis femoris* (L. cf) remains in proximity to the inner acetabular foramen without impinging upon the hyaline cartilage portion of the acetabulum cranially or the antitrochanter menisci caudally (Fig. 6C). However, the insertion of L. cf undergoes substantial dorsoventral deviation during the step cycle, appearing to be constrained by the inner acetabular foramen. The L. cf insertion deviates dorsally during the stance phase, whereas during the swing phase the L. cf insertion moves closer to one of the ligament's dual origins, or acetabular attachments. Specifically, the L. cf insertion approaches the origin site of the ligament's rostral crus, the *rostral ligamentum capitis femoris* (L. rcf), on the ischium's pubic peduncle. These deviations are consistent with cyclical changes in L. cf strain during the step cycle and are consistent among the three experimental animals (Supporting Information Fig. S1). The motion of the caudal crus, the *caudal ligamentum capitis femoris* (L. ccf), is excluded from this analysis due to its relatively smaller contribution to L. cf, as well as its attachment to the complex and likely mobile antitrochanter menisci. Although it is possible that the ligamentous linkage between the femur and the menisci may allow femoral movement to alter acetabular surface shape, modeling such motion is beyond the current capability of our methods.

Discussion

In this study, we used a combination of XROMM and contrast-enhanced CT techniques to elucidate the dynamic relationship between alligator hip joint soft tissues and surface regions during sustained forward terrestrial locomotion (high walking). We present articular relationships between the proximal femur and the acetabulum via particle traces and stroboscopic patch traces. Our results illustrate the utility of contrast-enhanced XROMM for assessing articular soft tissue interactions, and allow the proposal of functional hypotheses for crocodilian and archosaurian joint soft tissues based on their *in vivo* kinematic relationships.

Interpretation of soft tissue interpenetration

Throughout the step cycle, we observed instances in which articular soft tissue models on the femur interpenetrated substantially with those on the acetabulum. If all hip soft tissues were relatively rigid and accurately animated, we would expect close proximity and minimal interpenetration among articulating models. In all strides analyzed, we observe this relationship between the hyaline and fibrocartilage of the femoral head and the hyaline cartilage surrounding the pubo-iliac joint, which forms the rostral wall of the acetabulum. In contrast, the proximal femoral articular surface substantially and consistently interpenetrated with the models of the acetabular labrum and antitrochanter menisci. Because these instances appear cyclically across multiple strides and individuals, and only between certain structures, we consider them potential evidence of dynamic interactions among deformable tissues, rather than noise from tracking errors or filtering artifacts.
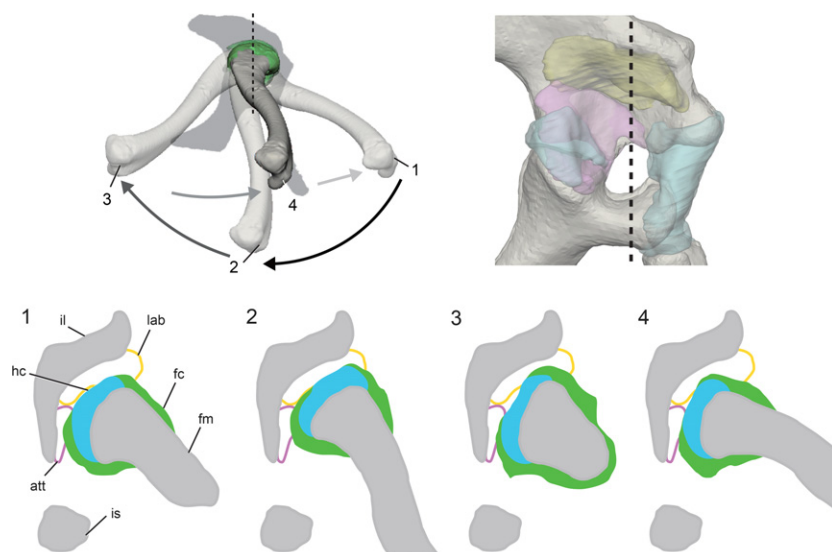
Acetabular labrum
In all strides analyzed that included mid-stance frames, the femoral hyaline cartilage surface penetrated the acetabular labrum model (yellow, Figs 3B and 5A). Because the acetabular labrum is composed of non-cartilaginous fibrous tissue that is appreciably more compliant than the hyaline cartilage core of the proximal femur (Tsai & Holliday, 2015), we infer that the proximal apex compressively deforms the acetabular labrum during these instances of interpenetration. Notably, when the hip joint is viewed in transverse section (Fig. 7), the profile of the proximal femur, and thus the shape of the space between it and the ilium, changes dramatically during the step cycle. Our interpenetration results do not reflect the actual magnitude of labrum deformation during each stride because the static *ex vivo* shape of the acetabular labrum cannot capture its dynamic *in vivo* shape.

Rather, the *in vivo* acetabular labrum is presumed to deform compressively to fit the space between the femur and the bony 'ceiling' of the acetabulum. Studies in mammals have suggested that the acetabular labrum functions to secrete and maintain a pressurized fluid layer within the hip joint (Ferguson et al. 1999), as well as provide a 'vacuum seal' to prevent synovial fluid flow away from the hip joint capsule (Terayama et al. 1980). Although the anatomical topology of the mammalian acetabular labrum differs from that of *Alligator*, we hypothesize that their common role as compressible articular structures on the external rim of the acetabular roof may indicate some similarity in function.

Antitrochanter menisci
Additionally, during late swing through early stance phases, the proximal hyaline cartilage surface interpenetrated with the antitrochanter model (purple, Figs 4B and 5A), indicative of dynamic soft tissue interactions at the posterior portion of the acetabulum. The antitrochanter consists of two fibrocartilaginous, overlapping menisci with ligamentous attachments to the acetabular labrum, the joint capsule, the bony acetabular surface, and the proximal femur itself (Tsai & Holliday, 2015). The presence of both collagen fibers and cartilaginous matrix suggests that the antitrochanter menisci may be less pliant than the acetabular labrum. However, the presence of extensive ligamentous attachments to the femur and other acetabular structures implies that the labrum may be able to slide and alter the shape of the posterior acetabulum depending on the relative position of the femur.

In humans and other mammals (Messner & Gao, 1998), the menisci in the knee joint serve to increase articular surface congruence between the distal femur and the tibial plateau. The human menisci shift posteriorly during knee flexion due to their ligamentous connection to the femur and tibia, thereby altering the shape of the articular surface

Fig. 7 Transverse sections of the femur and acetabulum at four positions during the high walk sequence (see Fig. 4). Sections taken at the black dashed line reveal that the available space for the deformable labrum (yellow) and mobile menisci (pink), between the much more rigid bone (gray) and femoral cartilages (blue and green), changes throughout the step cycle.

and maintaining congruence with the distal femur (Thompson et al. 1991). The antitrochanter menisci in the alligator hip joint may serve a similar function, and the interpenetration observed in the current study may be better interpreted as evidence of the menisci sliding around the proximal femur than as compressive deformation. Although the results of the current study are unable to detect the extent of acetabular shape changes and their potential effect on subsequent femoral movement, the dynamic relationship among antitrochanter position, overall acetabular shape, and femoral excursion remains an area worthy of further exploration.

The anatomical femoral head is not the functional femoral head

The majority of the anatomical femoral head remains lateral to the soft tissue limit of the acetabulum throughout much of the step cycle (Fig. 6A). At no point does the alligator's anatomical femoral head act as a stable pivot within the acetabulum. Rather, the entire terminal end of the alligator's proximal femur serves as the 'functional' femoral head.

Previous research on mammalian (MacLatchy & Bossert, 1996; Hammond et al. 2016) and avian (Baumel & Raikow, 1993; Martin & Ritchie, 1994; Kambic et al. 2014, 2015) hips has modeled the femoral head and acetabulum as a ball-and-socket articulation, in which the convex, sub-spherical femoral head rotates within a correspondingly shaped, concave acetabulum. In particular, avian hip joints are commonly modeled with the antitrochanter forming an additional physical contact between the femur and acetabulum, acting as a bony 'stop' that prevents femoral abduction and guides femoral axial rotation (Hertel et al. 2007). In contrast, the proximal femora of lepidosaurs and lissamphibians have been described as 'terminal' (Carroll, 1988; Kuznetsov & Sennikov, 2000), such that the proximal femur lacks a distinct 'head' region. Instead, the entire convex surface of the proximal femur articulates with the concave acetabulum. The evolution of the anatomical femoral head within the archosaurian radiation has received substantial attention in the comparative phylogenetic literature (Parrish, 1987b; Nesbitt, 2011). However, using the femoral head as a discrete, binary character has led postural reconstructions of fossil archosaurs to be based mainly on either mammals/birds, or lepidosaurs/lissamphibians, depending on the discretion of authors and museum exhibit designers (Hay, 1908; Tornier, 1909; Holland, 1910; Wade, 1989; Carpenter et al. 1994). Reconstructions of joint articulation directly influence range of motion estimates (Mallison, 2010b), joint pivot inferences (Langer, 2003), muscle moment arm calculations (Bates & Schachner, 2012), and bone loading (Blob, 2001). Therefore, it is crucial that joint articulation in fossil taxa is based upon shared anatomical and kinematic relationships between corresponding joint surfaces observed in their extant relatives.

Our results on hip articulation and kinematics of the American alligator question the applicability of using the anatomical femoral head for inferring the functional hip joint pivot in extinct archosaurs. Multiple lineages of archosaurs independently evolved sub-spherical, medially deflected anatomical femoral heads relative to the distal condyles (Carrano, 2000). Fossil archosaurs with such a distinct anatomical femoral head are often reconstructed such that the femoral head is oriented medially at 90° relative to the sagittal midline of the body and inserts directly into the acetabular fossa (e.g. *Allosaurus*, DMNH 2149; *Saturnalia*, Langer, 2003; *Plateosaurus*, Mallison, 2010a; but see Fechner, 2009 for alternative reconstruction on sauropodomorpha and Sereno & Arcucci, 1994 on basal dinosauromorpha). In taxa whose bony acetabular anatomy prevents the femoral head from inserting into the acetabulum at 90° (e.g. *Poposaurus*, Bates & Schachner, 2012), the femoral head is generally reconstructed in a craniomedially oriented, lepidosaur/lissamphibian-like position. Nevertheless, the avian-mammalian articulation scheme has been widely applied to *in silico* range-of-motion and biomechanical analyses of extinct archosaurian hind limbs (e.g. Hutchinson et al. 2005; Mallison, 2010a; Bates et al. 2012; Klinkhamer et al. 2018), in which the anatomical femoral head is assumed to function as a central pivot akin to a ball-and-socket articulation. The current study shows that even though the alligator possesses an anatomical femoral head recognizably offset from the femoral midshaft, the femur rotates via contact of the entire convex surface of the proximal femur against the acetabulum in a manner more similar to that observed in lepidosaurs (Snyder, 1989; Arnold et al. 2014).

Within the dinosaur lineage, early members of Theropoda (e.g. *Dilophosaurus*, Welles, 1984; *Tawa*, Nesbitt et al. 2009), Ornithischia (e.g. *Lesothosaurus*, Sereno, 1991a; *Eocursor*, Butler et al. 2007), and Sauropodomorpha (e.g. *Buriolestes*, Cabreira et al. 2016; *Macrocollum*, Müller et al. 2018) possess femora with craniomedially oriented femoral heads relative to the distal condyles, similar to those of crocodilians, rather than the medially oriented, sub-spherical femoral heads in more derived representatives of each respective clade (Hadrosauridae, Brett-Surman & Wagner, 2006; Sauropoda, Bonnan, 2004; Avetheropoda, Carrano et al. 2012). Additionally, the acetabulum of early dinosauromorphs shows osseous evidence of non-pivoting anatomical femoral heads similar to *Alligator* (Langer et al. 2010). In these taxa, the large, ventrolaterally descending supra-acetabular crest (inferred as a partially ossified iliofemoral ligament attachment by Tsai et al. 2018) prevents physical articulation of the anatomical femoral head with the acetabulum medially at 90° to the body's sagittal midline without impingement on the cartilage-covered femoral neck region. These lines of evidence are consistent with the femoral head in early dinosaur taxa inserting into

the acetabulum craniomedially, such that much or all of the proximal femur's terminal end facilitates articulation with the acetabulum, a condition more similar to crocodilians and lepidosaurs.

Our observations suggest that the presence, absence, or distinctiveness of the femoral head may not be the sole indicator of the central pivot of hip articulation in archosaurs, and that alligator-like, non-pivoting femoral heads may be more widespread among non-avian archosaurs. The inference of non-pivoting anatomical femoral heads in early saurischians suggests that in archosaurs, the anatomical femoral head likely evolved prior to the acquisition of its function as a central pivot of the femur within the acetabulum. Nevertheless, the independent, iterative evolution of sub-spherical, medially oriented femoral heads relative to the distal condyles within theropods, sauropodomorphs, and ornithischians (Carrano, 2000), as well as the multiple reductions of the bony supraacetabular crests (Tsai et al. 2018), likely signify independent shifts of the rotational pivot from the proximal femoral apex to the anatomical femoral head.

The femoral neck and antitrochanter maintain engagement during the stance phase of the step cycle

The femoral neck of *Alligator* maintains close proximity with the antitrochanter menisci during both stance and swing phases of high walk. Despite the femoral neck's continuity with the anatomical head on the convex proximal femur, kinematic traces of the alligator's femoral neck region resemble the expected kinematic behavior of the concave, saddle-shaped avian femoral neck (Fig. 6B). Studies on the femoral neck-antitrochanter articulation in birds have thus far focused primarily on *ex vivo* manipulations and modeling approaches (Hertel et al. 2007; Rankin et al. 2016), and it is generally agreed in the avian comparative literature that the antitrochanter undergoes physical overlap, or engagement, with the femoral neck during bipedal stance and terrestrial locomotion (Duff & Lynch, 1988; Abourachid et al. 2011).

However, the extent of femoral neck-antitrochanter engagement during *in vivo* femoral excursions, as well as the role of this articulation in bearing compressive loads, have been matters of contention among different authors. Hertel et al. (2007) and Hutchinson & Allen (2009) proposed that engagement of the antitrochanter with the femoral neck acts as an important load-bearing articulation, in addition to the femoral head-acetabular articulation. This view was contested by Goetz et al. (2008), who focused solely on the contact forces between the femoral head and the acetabulum during terrestrial locomotion of large palaeognaths and concluded that femoral neck-antitrochanter engagement does not bear any stance- or locomotor-induced loads. Martin & Ritchie (1994) characterized the hip

joints of non-cursorial birds as 'gliding hinges', wherein the antrochanter-femoral neck engagement presumably contributed to hip articulation. However, these authors also maintained that the hip joint of cursorial birds (e.g. 'ratites') acted more similar to ball-and-sockets, presumably with little contribution of antitrochanter-femoral neck engagement during normal terrestrial locomotion. Similarly, Bishop et al. (2018) proposed that the proximal femoral cancellous bone architecture of large non-avian theropods (e.g. *Allosaurus,* tyrannosaurids) indicated that these taxa also relied on the articulation between the sub-spherical femoral head region and the acetabular fossa as the primary hip articulation. However, these authors also suggested that articulation between the femoral neck and the ilial antitrochanter would have occurred occasionally. Disengagement of the avian femoral neck from the antitrochanter has thus far only been observed via *ex vivo* manipulation (Cracraft, 1971; Manafzadeh & Padian, 2018). It is therefore likely that the crocodilian hip joint also allows postures in which the femoral neck disengages from the antitrochanter dorsally, particularly during maximally extended hip postures as observed during swimming (Fish, 1984) and galloping (Zug, 1974; Webb & Gans, 1982). Nevertheless, our results indicate that during the high walk in *Alligator*, the femoral neck and antitrochanter maintain engagement throughout the step cycle.

Among extinct archosaurs, the antitrochanter leaves clear osteological correlates on the bony ilium and ischium in the form of laterally oriented subchondral surfaces of the ischial and ilial peduncle, respectively (Sereno, 1991b; Hutchinson, 2001b; Tsai et al. 2018). Correspondingly, a continuous layer of articular cartilage can be inferred to have been present on both the anatomical femoral head and femoral neck regions in many extinct archosaurs, as indicated by the uninterrupted subchondral growth plate surface on the proximal femur (Hutchinson, 2001b). Both the antitrochanter and the cartilaginous femoral neck are anatomical characters shared among extant archosaurs (Tsai & Holliday, 2015), and the kinematic patterns of femoral neck-antitrochanter engagement in *Alligator* during the high walk in this study greatly mirror the condition inferred for extant birds. Therefore, we hypothesize that engagement between the femoral neck and the antitrochanter articulation during terrestrial locomotion is likely a conserved aspect of hip joint articulation among archosaurs.

The inner acetabular foramen constrains the femoral head ligament

The inner acetabular walls of birds and crocodilians are unossified and form an acetabular foramen within the surrounding pelvic bones, bounded internally by an acetabular membrane during life. The acetabular membrane serves as the medial boundary of the acetabulum (Tsai & Holliday, 2015). By tracing the motion path left by the femoral

insertion of L. cf during terrestrial locomotion, we show that the alligator L. cf remains lateral to the acetabular foramen, without craniocaudal impingement between the femoral and acetabular surfaces (Fig. 6C). The anatomical arrangement of L. cf in *Alligator* and this ligament's kinematic relationship with the acetabular membrane resemble the condition in birds. The avian L. cf attaches from the ventral rim of the inner acetabular foramen to the fovea capitis of the anatomical femoral head (Martin et al. 1994) and remains between the femoral head and the inner acetabular membrane throughout normal *in vivo* femoral postures (MacCoy, 1989). Our results therefore suggest that the acetabular foramen of archosaurs forms a concave region within the acetabulum to accept L. cf, thereby preventing impingement.

Whereas the avian L. cf binds the femoral head tightly inside the acetabulum (Martin, et al. 1994), the crocodilian L. cf is here inferred to allow substantially more mobility between its attachment sites. The femoral insertion of the alligator's L. cf undergoes dorsoventral movement during each step of the high walk, suggesting cyclical stretching during each load-bearing phase. Although it is not possible directly to observe L. cf. during crocodilian terrestrial locomotion, our kinematic results allow us to infer that the bony boundaries of the inner acetabular foramen constrain L. cf movement in *Alligator*. This proposed function is analogous to that of the acetabular notch in mammals, a fat-filled cavity within the acetabular fossa that houses the *ligamentum teres femoris* (Beltran et al. 1986; Fuss & Bacher, 1991) and prevents its impingement between femoral- and acetabular lunate surface during femoral excursions. Although the structural homology of the archosaurian L. cf and the mammalian *ligamentum teres* has not yet been explored in the comparative literature, our results nevertheless suggest that the presence of a hollowed cavity lined with pliant soft tissues within the acetabular fossa is the osteological correlate for the presence of an intracapsular ligament in the hip joint.

Unossified inner acetabular walls, commonly referred to as 'perforate acetabulum' (Romer, 1956), were recognized by Novas (1996) as a synapomorphy of Dinosauria. Subsequent work by Langer & Benton (2006) indicated that the initial bony aperture in the inner acetabular wall is relatively small compared with the bony acetabulum in basal theropods, ornithopods, and sauropodomorphs. This observation suggests that enlargements of the inner acetabular foramen occurred in parallel in the dinosaurian clades. Bakker & Galton (1974) suggested that the perforate acetabulum is a mechanical consequence during the evolution of adducted hip posture in archosaurs, such that the decrease in medially directed ground reaction forces favors the reduction, and eventual loss, of bony inner acetabular walls. Egawa et al (2018) further investigated the developmental mechanism of acetabular perforation in the avian hip joint, and proposed that the evolution of a membranous inner acetabular wall in dinosaurs resulted from the loss of cartilaginous anlagen at the inner acetabular wall during embryogenesis. Presence of a perforate acetabulum has thus been used by numerous authors (Sereno, 1991a; Kubo & Benton, 2007; Brusatte et al. 2010) as an indicator of adducted hind limb postures in archosaurs. These postural inferences based on acetabular perforation do not necessarily contradict our inference of acetabular perforation as an osteological correlate for intracapsular ligaments. However, it is noteworthy that the perforate acetabulum does not preclude *Alligator* from assuming abducted hind limb postures during resting and low walk behaviors. Nevertheless, the femoral attachment of L. cf remains in proximity to the inner acetabular foramen in both *Alligator* and birds. Therefore, these osseous features may be useful for constraining hip range of motion in extinct archosaurs, such that postures which result in craniocaudal deviation of the two sites can be excluded on the basis of potential ligamentous impingement.

Femoral soft tissue arrangement and interaction in the alligator hip joint

The femoral hyaline cartilage surface moves substantially during the step cycle, but remains largely restricted to the confines of acetabular tissues (Fig. 5A). The extent of spatial overlap between the two articular surfaces may be explained by the potential load-bearing function of the femoral hyaline cartilage. Research on mammalian cartilaginous tissues indicates that hyaline cartilage is more resistant to compressive loads (Yamada, 1970; Benjamin & Evans, 1990), whereas fibrocartilage is more resistant to tensile and shear loads (Freemont & Hoyland, 2006). Regional differences in loading modality have been demonstrated in the limb joints of humans (Afoke et al. 1987; Assassi & Magnenat-Thalmann, 2014) and domestic dogs (O'Connor et al. 1988), suggesting that the alligator hip joint may experience regional differences in the magnitudes of compressive and shear loads as well.

Although the material properties of crocodilian hyaline and fibrocartilage are not known, assuming they are similar to those of mammals, we propose a functional explanation for the arrangement of proximal femoral articular soft tissues in light of their observed dynamic interactions with the acetabulum. Constraining the movements of the hyaline cartilage within the acetabulum during terrestrial locomotion, particularly during the stance phase, is consistent with the assumption that the hyaline cartilage portion of the alligator's proximal femur is more resistant to compressive loading than the fibrocartilage portion. Indeed, we observed that the hyaline cartilage surface engages the soft, readily deformable acetabular labrum between mid-stance and late-stance phases, during which the animal pushes its hind limb caudoventrally against the substrate in order to propel the body forward.

Alternatively, if the material properties of crocodilian hyaline and fibrocartilage do not differ significantly from one another, then the observed dynamic interaction between the femoral hyaline cartilage and the acetabulum may require another explanation. Nevertheless, the observed motion pattern suggests that the articular soft tissue border of the acetabulum and the fibro-hyaline cartilage junction may be informative for describing the range of achievable femoral positions during the high walk, as the extent of the proximal femoral hyaline cartilage remains in articulation with the acetabular soft tissues.

Although the extent of femoral hyaline cartilage and acetabular soft tissues may be predictive of femoral positions during the high walk, the topography of these soft tissues may be less informative for inferring joint poses outside of the high walk posture, including the maximum active or passive range of hip joint motion. Crocodilians are able voluntarily to hyperextend the hip joints during hind limb-propelled jumps from solid substrates (Targarona et al. 2010), as well as during swimming behaviors, in which the hind limbs are held close to the tail in order for the body to undulate laterally while maintaining a streamlined contour (Seebacher et al. 2003). During hip hyperextension, the femoral hyaline cartilage surface would likely travel beyond the cranioventral border of the acetabular soft tissues. This hypothesis remains to be tested using additional kinematic data from non-high walk behaviors.

Acknowledgements

Conflict of interest

The authors declare no conflicts of interest in preparing this article.

Author contributions

H.P.T. conceived the study. S.M.G. and H.P.T. designed the study. H.P.T., S.M.G., M.L.T., and A.R.M. carried out the experiments and analyses. H.P.T. drafted the manuscript, with critical evaluation and approval for submission by M.L.T., A.R.M., and S.M.G.

Data availability

The XROMM raw footage, calibration trials, and CT scan-derived surface models used in this study are available on the X-Ray Motion Analysis Research Portal (http://xmaportal.org).

References

Abourachid A, Hackert R, Herbin M, et al. (2011) Bird terrestrial locomotion as revealed by 3D kinematics. *Zoology* **114**, 360–368.

Afoke NY, Byers PD & Hutton WC (1987) Contact pressures in the human hip joint. *J Bone Joint Surg Br* **69**, 536–541.

Arnold P, Fischer MS, Nyakatura JA (2014) Soft tissue influence on ex vivo mobility in the hip of *Iguana*: Comparison with in vivo movement and its bearing on joint motion of fossil sprawling tetrapods. *J Anat* **225**, 31–41.

Assassi L & Magnenat-Thalmann N (2014) A biomechanical approach for dynamic hip joint analysis. In: *3D Multiscale Physiological Human* (eds Magnenat-Thalmann N, Ratib O, Choi HF), pp. 233–252. London: Springer.

Bakker RT, Galton PM (1974) Dinosaur monophyly and a new class of vertebrates. *Nature* **248**, 168.

Bates KT & Schachner ER (2012) Disparity and convergence in bipedal archosaur locomotion. *J R Soc Interface* **9**, 1339–1353.

Bates KT, Benson RBJ, Falkingham PL (2012) A computational analysis of locomotor anatomy and body mass evolution in Allosauroidea (Dinosauria: Theropoda). *Paleobiology* **38**, 486–507.

Baumel JJ & Raikow RJ (1993) Arthrologia. In: *Handbook of Avian Anatomy: Nomina Anatomica Auium.* (eds Baumel JJ, King AS, Breazile JE et al.), pp. 133–187, Cambridge: Nuttall Ornithological Club.

Baumel JJ & Witmer LM (1993) Osteologia. In: *Handbook of Avian Anatomy: Nomina Anatomica Auium.* (eds Baumel JJ, King AS, Breazile JE et al.), pp. 45–132, Cambridge: Nuttall Ornithological Club.

Beltran J, Noto AM, Herman LJ, et al. (1986) Joint effusions: MR imaging. *Radiology* **158**, 133–137.

Benjamin M & Evans EJ (1990) Fibrocartilage. *J Anat* **171**, 1–15.

Benson RBJ, Choiniere JN (2013) Rates of dinosaur limb evolution provide evidence for exceptional radiation in Mesozoic birds. *Proc Biol Sci* **280**, 20131780.

Bishop PJ, Hocknull SA, Clemente CJ, et al. (2018) Cancellous bone and theropod dinosaur locomotion. Part II-a new approach to inferring posture and locomotor biomechanics in extinct tetrapod vertebrates. *PeerJ* **6**, e5779.

Blob RW (2001) Evolution of hindlimb posture in nonmammalian therapsids: biomechanical tests of paleontological hypotheses. *Paleobiology* **27**, 14–38.

Bonnan MF (2004) Morphometric analysis of humerus and femur shape in Morrison sauropods: implications for functional morphology and paleobiology. *Paleobiology* **30**, 444–470.

Bonnan MF, Sandrik JL, Nishiwaki T, et al. (2010) Calcified cartilage shape in archosaur long bones reflects overlying joint shape in stress-bearing elements: implications for nonavian dinosaur locomotion. *Anat Rec* **293**, 2044–2055.

Brainerd EL, Baier DB, Gatesy SM, et al. (2010) X-ray reconstruction of moving morphology (XROMM): precision, accuracy and applications in comparative biomechanics research. *J Exp Zool A Ecol Genet Physiol* **313**, 262–279.

Brett-Surman MK & Wagner JR (2006) Discussion of character analysis of the appendicular anatomy in Campanian and Maastrichtian North American hadrosaurids-variation and ontogeny. In: *Horns and Beaks: Ceratopsian and Ornithopod Dinosaurs*(ed. Carpenter K), pp. 135–169. Bloomington: Indiana University Press.

Brinkman D (1980) The hind limb step cycle of *Caiman sclerops* and the mechanics of the crocodile tarsus and metatarsus. *Can J Zool* **58**, 2187–2200.

Brusatte SL, Benton MJ, Desojo JB, et al. (2010) The higher-level phylogeny of Archosauria (Tetrapoda: Diapsida). *J Syst Palaeontol* **8**, 3–47.

Butler RJ, Smith RMH & Norman DB (2007) A primitive ornithischian dinosaur from the Late Triassic of South Africa, and the early evolution and diversification of Ornithischia. *Proc Biol Sci* **274**, 2041–2046.

Cabreira SF, Kellner AWA, Dias-da-Silva S, et al. (2016) A unique late triassic dinosauromorph assemblage reveals dinosaur ancestral anatomy and diet. *Curr Biol* **26**, 3090–3095.

Carpenter K, Madsen JH & Lewis A (1994) Mounting of fossil vertebrate skeletons. In: Leiggi P & May P, eds, Vertebrate Paleontological Techniques, Vol. 1, pp. 228–322. New York: Cambridge University Press.

Carrano MT (2000) Homoplasy and the evolution of dinosaur locomotion. *Paleobiology* **26**, 489–512.

Carrano MT, Benson RBJ & Sampson SD (2012) The phylogeny of Tetanurae (Dinosauria: Theropoda). *J Syst Palaeontol* **10**, 211–300.

Carroll RL (1988) *Vertebrate Paleontology and Evolution*. New York: W. H. Freeman and Co.

Coombs WP (1975) Sauropod habits and habitats. *Palaeogeogr Palaeoclimatol Palaeoecol* **17**, 1–33.

Cracraft J (1971) The functional morphology of the hind limb of the domestic pigeon, *Columba livia*. *Bull Am Mus Nat Hist* **144**, 175–268.

Dilkes DW (2001) An ontogenetic perspective on locomotion in the Late Cretaceous dinosaur *Maiasaura peeblesorum* (Ornithischia: Hadrosauridae). *Can J Earth Sci* **38**, 1205–1227.

Duff SR & Lynch M (1988) Antitrochanteric and acetabular lesions in adult male breeding turkeys. *Avian Pathol* **17**, 121–137.

Egawa S, Saito D, Abe G, et al. (2018) Morphogenetic mechanism of the acquisition of the dinosaur-type acetabulum. *R Soc Open Sci* **5**, 180604.

Fechner R (2009) Morphofunctional evolution of the pelvic girdle and hindlimb of Dinosauromorpha on the lineage to Sauropoda. Doctoral. Ludwigs Maximilians Universitat, Munchen. Available: https://edoc.ub.uni-muenchen.de/10954/1/Fechner_Regina.pdf

Ferguson SJ, Bryant JT & Ito K (1999) An investigation of the function of the acetabular labrum using a poroelastic finite element model. *J Bone Joint Surg Br* **81**, 69.

Fish FE (1984) Kinematics of undulatory swimming in the American alligator. *Copeia* **1984**, 839–843.

Freemont AJ & Hoyland J (2006) Lineage plasticity and cell biology of fibrocartilage and hyaline cartilage: its significance in cartilage repair and replacement. *Eur J Radiol* **57**, 32–36.

Fujiwara S-I, Taru H & Suzuki D (2010) Shape of articular surface of crocodilian (Archosauria) elbow joints and its relevance to sauropsids. *J Morphol* **271**, 883–896.

Fuss FK, Bacher A (1991) New aspects of the morphology and function of the human hip joint ligaments. *Am J Anat* **192**, 1–13.

Gadow H (1901) *Amphibia and Reptiles*. London: Macmillan and Company Ltd.

Galton P (1969) The pelvic musculature of the dinosaur Hysilophodon (Reptilia: Ornithischia). *Postilla* **131**, 1–64.

Gatesy SM (1991) Hind limb movements of the American alligator (*Alligator mississippiensis*) and postural grades. *J Zool* **224**, 577–588.

Gatesy SM, Middleton KM (1997) Bipedalism, flight, and the evolution of theropod locomotor diversity. *J Vert Paleontol* **17**, 308–329.

Gignac PM, Kley NJ, Clarke JA, et al. (2016) Diffusible iodine-based contrast-enhanced computed tomography (diceCT): an emerging tool for rapid, high-resolution, 3-D imaging of metazoan soft tissues. *J Anat* **228**, 889–909.

Gilmore CW (1914) Osteology of the armored Dinosauria in the United States National museum: with special reference to the genus *Stegosaurus*. *Bull Am Mus Nat Hist* **89**, 1–143.

Goetz JE, Derrick TR, Pedersen DR, et al. (2008) Hip joint contact force in the emu (*Dromaius novaehollandiae*) during normal level walking. *J Biomech* **41**, 770–778.

Hammond AS, Plavcan JM & Ward CV (2016) A validated method for modeling anthropoid hip abduction in silico. *Am J Phys Anthropol* **160**, 529–548.

Hay OP (1908) On the habits and the pose of the sauropodous dinosaurs, especially of *Diplodocus*. *Am Nat* **42**, 672–681.

Hertel F, Campbell KE, James HF (2007) The antitrochanter of birds: form and function in balance. *Auk* **124**, 789–805.

Holland WJ (1910) A review of some recent criticisms of the restorations of sauropod dinosaurs existing in the museums of the United States, with special reference to that of *Diplodocus carnegiei* in the Carnegie Museum. *Am Nat* **44**, 258–283.

Holliday CM, Ridgely RC, Sedlmayr JC, et al. (2010) Cartilaginous epiphyses in extant archosaurs and their implications for reconstructing limb function in dinosaurs. *PLoS One* **5**, 0013120.

Hutchinson J (2001a) The evolution of femoral osteology and soft tissues on the line to extant birds (Neornithes). *Zool J Linn Soc* **131**, 169–197.

Hutchinson JR (2001b) The evolution of pelvic osteology and soft tissues on the line to extant birds (Neornithes). *Zool J Linn Soc* **131**, 123–168.

Hutchinson JR & Allen V (2009) The evolutionary continuum of limb function from early theropods to birds. *Naturwissenschaften* **96**, 423–448.

Hutchinson JR, Anderson FC, Blemker SS, et al. (2005) Analysis of hindlimb muscle moment arms in *Tyrannosaurus rex* using a three-dimensional musculoskeletal computer model: implications for stance, gait, and speed. *Paleobiology* **31**, 676–701.

Huxley TH (1870) Further evidence of the affinity between the dinosaurian reptiles and birds. *Q J Geol Soc London* **26**, 12–31.

Jeffery NS, Stephenson RS, Gallagher JA, et al. (2011) Micro-computed tomography with iodine staining resolves the arrangement of muscle fibres. *J Biomech* **44**, 189–192.

Kambic RE, Roberts TJ & Gatesy SM (2014) Long-axis rotation: a missing degree of freedom in avian bipedal locomotion. *J Exp Biol* **217**, 2770–2782.

Kambic RE, Roberts TJ & Gatesy SM (2015) Guineafowl with a twist: asymmetric limb control in steady bipedal locomotion. *J Exp Biol* **218**, 3836–3844.

Klinkhamer AJ, Mallison H, Poropat SF, et al. (2018) Three-dimensional musculoskeletal modeling of the sauropodomorph hind limb: the effect of postural change on muscle leverage. *Anat Rec* **301**, 2145–2163.

Knörlein BJ, Baier DB, Gatesy SM, et al. (2016) Validation of XMALab software for marker-based XROMM. *J Exp Biol* **219**, 3701–3711.

Kubo T & Benton MJ (2007) Evolution of hindlimb posture in archosaurs: limb stresses in extinct vertebrates. *Palaeontology* **50**, 1519–1529.

Kuznetsov AN & Sennikov AG (2000) On the function of a perforated acetabulum in archosaurs and birds. *Paleontol J (Paleontologicheskii zhurnal)* **34**, 439–448.

Lacerda MB, Mastrantonio BM, Fortier DC, et al. (2016) New insights on *Prestosuchus chiniquensis* Huene, 1942 (Pseudosuchia, Loricata) based on new specimens from the 'Tree Sanga' Outcrop, Chiniquá Region, Rio Grande do Sul, Brazil. *PeerJ* **4**, e1622.

Langer MC (2003) The pelvic and hind limb anatomy of the stem-sauropodomorph *Saturnalia tupiniquim* (Late Triassic, Brazil). *PaleoBios* **23**, 1–30.

Langer MC, Benton MJ (2006) Early dinosaurs: a phylogenetic study. *J Syst Palaeontol* **4**, 309–358.

Langer MC, Bittencourt JS & Schultz CL (2010) A reassessment of the basal dinosaur *Guaibasaurus candelariensis*, from the late triassic caturrita formation of south Brazil. *Earth Environ Sci Trans R Soc Edinb* **101**, 301–332.

Lehman TM (1989) *Chasmosaurus mariscalensis*, sp. nov., a new ceratopsian dinosaur from Texas. *J Vert Paleontol* **9**, 137–162.

MacCoy DM (1989) Excision arthroplasty for management of coxofemoral luxation in pet birds. *J Am Vet Med Assoc* **194**, 95–97.

MacLatchy LM & Bossert WH (1996) An analysis of the articular surface distribution of the femoral head and acetabulum in anthropoids, with implications for hip function in Miocene hominoids. *J Hum Evol* **31**, 425–453.

Maidment SCR & Barrett PM (2012) Does morphological convergence imply functional similarity? A test using the evolution of quadrupedalism in ornithischian dinosaurs. *Proc R Soc B* **279**, 3765–3771.

Mallison H (2010a) The digital *Plateosaurus* I: body mass, mass distribution, and posture assessed using CAD and CAE on a digitally mounted complete skeleton. *Palaeontol Electronica* **13**, 8.

Mallison H (2010b) *CAD assessment of the posture and range of motion of Kentrosaurus aethiopicus* Hennig 1915. *Swiss J Geosci* **103**, 211–233.

Manafzadeh AR & Padian K (2018) ROM mapping of ligamentous constraints on avian hip mobility: implications for extinct ornithodirans. *Proc R Soc Lond B* **285**, 20180727.

Marsh OC (1896) The Dinosaurs of North America, U.S. Government Printing Office. United States Geological Survey 16th Annual Report 1894–1895: 133–244.

Martin H & Ritchie BW (1994) Orthopedic Surgical Techniques. In: *Avian Medicine: Principles and Application* (eds Ritchie BW, Harrison GJ, Harrison LR), pp. 1139–1169. Lake Worth: Wingers Pub.

Martin HD, Kabler R & Sealing L (1994) The avian coxofemoral joint: a review of regional anatomy and report of an open-reduction technique for repair of a coxofemoral luxation. *J Assoc Avian Vet* **8**, 164–172.

Messner K & Gao J (1998) The menisci of the knee joint. Anatomical and functional characteristics, and a rationale for clinical treatment. *J Anat* **193** (Pt 2), 161–178.

Metscher BD (2009) MicroCT for comparative morphology: simple staining methods allow highcontrast 3D imaging of diverse non-mineralized animal tissues. *BMC Physiol* **9**, 11.

Müller RT, Langer MC & Dias-da-Silva S (2018) An exceptionally preserved association of complete dinosaur skeletons reveals the oldest long-necked sauropodomorphs. *Biol Lett* **14**, 20180633.

Nesbitt SJ (2011) The early evolution of archosaurs: relationships and the origin of major clades. *Bull Am Mus Nat Hist* **352**, 1–292.

Nesbitt SJ, Smith ND, Irmis RB, et al. (2009) A complete skeleton of a Late Triassic saurischian and the early evolution of dinosaurs. *Science* **326**, 1530–1533.

Novas FE (1996) Dinosaur monophyly. *J Vert Paleontol* **16**, 723–741.

O'Connor P, Orford CR & Gardner DL (1988) Differential response to compressive loads of zones of canine hyaline articular cartilage: micromechanical, light and electron microscopic studies. *Ann Rheum Dis* **47**, 414–420.

Osborn HF (1898) Additional characters of the great herbivorous dinosaur *Camarasaurus*. *Bull Am Mus Nat Hist* **10**, 219–233.

Parrish JM (1987a) Locomotor adaptations in the hindlimb and pelvis of the Thecodontia. *Hunteria* **1**, 1–35.

Parrish JM (1987b) The origin of crocodilian locomotion. *Paleobiology* **13**, 396–414.

Pauwels E, Van Loo D, Cornillie P, et al. (2013) An exploratory study of contrast agents for soft tissue visualization by means of high resolution X-ray computed tomography imaging. *J Microsc* **250**, 21–31.

Rankin JW, Rubenson J & Hutchinson JR (2016) Inferring muscle functional roles of the ostrich pelvic limb during walking and running using computer optimization. *J R Soc Interface* **13**, pii: 20160035.

Reilly SM & Elias JA (1998) Locomotion in *Alligator mississippiensis*: kinematic effects of speed and posture and their relevance to the sprawling-to-erect paradigm. *J Exp Biol* **201**(Pt 18), 2559–2574.

Romer AS (1923) The pelvic musculature of saurischian dinosaurs. *Bull Am Mus Nat Hist* **48**, 605–617.

Romer AS (1956) *Osteology of the Reptiles*. Chicago: University of Chicago Press.

Rubenson J, Lloyd DG, Besier TF, et al. (2007) Running in ostriches (*Struthio camelus*): three-dimensional joint axes alignment and joint kinematics. *J Exp Biol* **210**, 2548–2562.

Sawin HJ (1947) The pseudosuchian reptile *Typothorax meadei*. *J Paleontol* **21**, 201–238.

Seebacher F, Elsworth PG & Franklin CE (2003) Ontogenetic changes of swimming kinematics in a semi-aquatic reptile (*Crocodylus porosus*). *Aust J Zool* **51**, 15–24.

Sereno PC (1991a) *Lesothosaurus*, 'Fabrosaurids', and the early evolution of ornithischia. *J Vert Paleontol* **11**, 168–197.

Sereno PC (1991b) Basal archosaurs: phylogenetic relationships and functional implications. *J Vert Paleontol* **11**, 1–53.

Sereno PC & Arcucci AB (1994) Dinosaurian precursors from the Middle Triassic of Argentina: *Lagerpeton chanarensis*. *J Vert Paleontol* **13**, 385–399.

Snyder RC (1954) The anatomy and function of the pelvic girdle and hindlimb in lizard locomotion. *Am J Anat* **95**, 1–45.

Targarona RR, Soberón RR, Tabet MA, et al.(2010) Cuban crocodile (*Crocodylus rhombifer*). In: *Crocodiles: Status, Survey and Conservation Action Plan*, 3rd edn. (ed. Manolis SC), pp. 114–118, Darwin: Crocodile Specialist Group.

Terayama K, Takei T & Nakada K (1980) Joint space of the human knee and hip joint under a static load. *Eng Med* **9**, 67–74.

Thompson WO, Thaete FL, Fu FH, et al. (1991) Tibial meniscal dynamics using three-dimensional reconstruction of magnetic resonance images. *Am J Sports Med* **19**, 210–216.

Tornier G (1909) Wie war der *Diplodocus carnegii* wirklich gebaut. *Sitzungsbericht der Gesellschaft naturforschender Freunde zu Berlin* **4**, 193–209.

Tsai HP, Holliday CM (2011) Ontogeny of the alligator cartilago transiliens and its significance for sauropsid jaw muscle evolution. *PLoS One* **6**, e24935.

Tsai HP & Holliday CM (2015) Articular soft tissue anatomy of the archosaur hip joint: Structural homology and functional implications. *J Morphol* **276**, 601–630.

Tsai HP, Middleton KM, Hutchinson JR, et al. (2018) Hip joint articular soft tissues of non-dinosaurian Dinosauromorpha and early Dinosauria: evolutionary and biomechanical implications for Saurischia. *J Vert Paleontol* **38**, e1427593.

Wade M (1989) The stance of dinosaurs and the Cossack dancer syndrome. In: *Dinosaur Tracks and Traces* (eds Gillette DD & Lockley MG), pp. 73–82. Cambridge: Cambridge University Press.

Webb GJW, Gans C (1982) Galloping in *Crocodylus johnstoni* – a reflection of terrestrial activity? *Rec Aust Mus* **34**, 607–618.

Welles SP (1984) *Dilophosaurus wetherilli* (Dinosauria, Theropoda) osteology and comparisons. Palaeontogr Abt A Band A185. *Lieferung* **185**, 85–180.

Wilson JA, Carrano MT (1999) Titanosaurs and the origin of "wide-gauge" trackways: a biomechanical and systematic perspective on sauropod locomotion. *Paleobiology* **25**, 252–267.

Yamada H (1970) *Strength of Biological Materials* (ed. Evans G). Baltimore: Williams & Wilkins.

Zug GR (1974) Crocodilian galloping: an unique gait for reptiles. *Copeia* **1974**, 550–552.

Supporting Information

Additional Supporting Information may be found in the online version of this article:

Figure S1. Comparison among the insertion sites of L. cf as marked on the proximal femora of the three experimental animals (top row, all in medial view), as well as the stroboscopic patch traces left by the L.cf insertion site in the bony acetabula during multiple high walk sequences (bottom row, all in lateral view).

Video S1. Stroboscopic patch traces of proximal femoral regions relative to the acetabulum during a typical high-walking stride (Animal 3, Run 1) slowed to 1/10th speed.